Low loss silica waveguides containing Si nanocrystals

C. Garcia[1], B. Garrido[1], P. Pellegrino[1], J.R. Morante[1], M. Melchiorri[2], N. Daldosso[2], L. Pavesi[2], E. Scheid[3], G. Sarrabayrouse[3]
[1]Electronics, University of Barcelona, Barcelona, Spain;
[2]Physics, University of Trento, Trento, Italy;
[3]LAAS - CNRS, Toulouse, France;

ABSTRACT

We study the optical and structural properties of rib-loaded waveguides working in the 600-900 nm spectral range. A Si nanocrystal-rich SiO_x with Si excess nominally ranging from 10 to 20% forms the active region of the waveguide. Starting materials were fused silica wafers and 2 μm-thick SiO_2 thermally grown onto Si substrate. Si nanocrystals were precipitated by annealing at 1100ºC after quadruple Si ion implantation to high doses in a flat profile. The complete phase separation and formation of Si nanocrystals were monitored by means of optical tools, such as Raman, optical absorption and photoluminescence. Grain size distribution was obtained by electron microscopy. The actual Si excess content was obtained by X-ray photoelectron spectroscopy. The rib-loaded structure of the waveguide was fabricated by photolitographic and reactive ion etching processes, with patterned rib widths ranging from 1 to 8 μm. M-lines spectroscopy measurements provided a direct measurement of the refractive index and thickness of the active layers versus Si excess. When coupling a probe signal at 780 nm or 633 nm into the waveguide, an attenuation of at least 11 dB/cm was observed. These propagation losses have been attributed to Mie scattering, waveguide irregularities and direct absorption by the silicon nanocrystals.

INTRODUCTION

Si nanocrystals in amorphous matrices have been subject of intensive studies as a suitable optical active medium for CMOS-compatible photonic applications. The optical and structural properties of nanostructured silicon have been exhaustively investigated, and are relatively well understood [1, 2]. More recently, the important observation of optical gain from nanocrystalline Si has been reported [3, 4]. In this contribution we focus the attention in analysing the loss mechanisms in waveguide structures built with this material.

EXPERIMENTAL DETAILS

In order to introduce Si excess inside the oxide matrix, multiple Si^+ ion implantations have been performed in both 2 μm thick SiO_2 films thermally grown on Si and pure fused quartz wafers. Ion energies and relative doses of the multiple implantations were chosen to give rise to a "box-like" Si super-saturation down to a depth of about 0.4 μm. In such a way, the processing of the layers will allow to fabricate channel waveguides with a well defined homogeneous in-depth active media providing refractive index contrast with the claddings. The total ion doses were tailored to introduce a Si excess nominally ranging from 10% to 20% referred to the silica atomic concentration before implantation. Then the samples were annealed at 1100 ºC in N_2 atmosphere for different durations, ranging from 1 min up to 16 h.

Conventional Transmission Electron Microscopy (TEM) in dark field was used to image the different multilayer structure, while Energy-Filtered TEM (EFTEM) was employed to monitor the size distribution of nanocrystals and its evolution with the implanted dose. Systematic photo-luminescence (PL) measurements were performed in all samples by using an Ar laser for ultra-violet excitation at 365 nm. The luminescent emission was analysed in backscattering mode by a 0.6 m monochromator and detected with a GaAs Hamamatsu photomultiplier.

The rib-loaded waveguides (WGs) have been first modelled, using the experimentally determined refractive index of the active layer. Simulations were performed in order to ensure that the chosen geometry allows the propagation inside the active layer with a good confinement factor. A set of rib widths was considered, with rib widths ranging from 1 to 8 µm, with over 65% of the energy confined inside the active layer. Simulations also proved that the WGs supported only the fundamental mode for rib widths under 4 µm, and started being multimode after that.

A 1µm-thick PECVD SiO_2 layer was deposited over the 4" wafer with the 15% nominal (9.5% measured) Si excess. Deposition was performed at 300 ºC. Ridge structures were then formed in this layer by using standard photolithography and reactive ion etching to a depth of 0.7µm. An unetched cladding layer of 0.3µm was preserved, partly to act as a protection and partly to ensure single mode behaviour and mode symmetry. The mask used in the photolithographic process was patterned with 1 cm^2 squares, each containing eight groups of waveguides 1 to 8 µm-wide, separated by 240 µm in order to ensure proper mode isolation.

The waveguides have been characterized by coupling-in visible light from a laser (780nm – about 7 mW; 633nm – few mW) through a tapered fiber and coupling-out the light with a microscope objective (40x) matched to a zoom mounted on a high performance CCD camera. Top-view observation has been performed by means of an optical microscope and a CCD camera mounted on top of the measuring system. A prism beam splitter allows splitting the transmitted light in two parts: one is directed to the CCD camera, the other is directed to a calibrated photodiode, which yields power measurement of the transmitted light.

DISCUSSION

To characterize the material used to fabricate the waveguides, several experimental techniques have been employed. A typical dark field TEM picture of the Si-nanocrystal-rich layer, overlapped with the Si ion implanted profile as obtained by SIMS is shown in Fig. 1. From these measurements, the thickness of the implanted layer has been estimated to be around 300 nm, independent on the implanted ion dose. XPS analysis provides a quantitative evaluation of the silicon and oxygen content inside the implanted region, and then a direct measure of the introduced Si excess. For the three implantation schemes, a Si excess of 13, 9.5 and 7% have been found for the nominal 20, 15 and 10%, respectively. The variation with respect to the expected values, calculated with the help of the SRIM simulator, can be mainly assigned to the expansion of the layer to accommodate a number of ions, which is comparable to the number of target atoms. A further refinement of the calculation, including swelling of the implanted layers, brings to an almost perfect agreement between the measured and the calculated values.

The thermal evolution of the implanted silicon ions have been followed after each annealing step by means of Raman and visible absorption measurements. In all the as-implanted samples the Raman spectrum is dominated by a broad structure peaked around 480 cm^{-1}, signature of the transverse optical mode of amorphous Si aggregates. From the similarity of areas under the Raman bands before and after annealing we can conclude that most of the Si excess is already

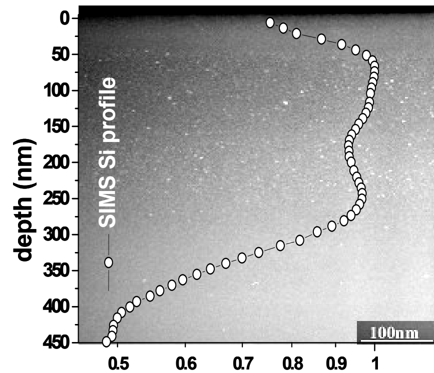

Figure 1. SIMS profile of the implanted silicon as a function of sample depth. The nanocrystal-rich layer, as observed in dark-field TEM, clearly overlaps with the flat implantation.

clustered in amorphous aggregates even in the as-implanted state. After annealing the wafers at 1100 ºC for 20 minutes, the Raman spectrum is converted into a narrow asymmetric peak centred at about 521 cm^{-1}, indicating a rapid and complete crystallization of the amorphous clusters. Further annealing at the same temperature does modify neither the shape nor the intensity of the Si crystalline signal. Moreover, the integrated signal of the crystalline Si peak perfectly scales with the implanted dose. Similar results have been obtained from optical transmission in the whole visible range: the absorption spectrum is essentially the same for all the samples, once rescaled to the implanted dose, and it does not change after 20 min. annealing. We can then infer that the crystalline fraction of precipitated Si is proportional to the implanted dose and for an annealing step of only 20' at 1100 ºC a complete crystallization occurs.

By varying the implanted dose a change in the average size and density of precipitated nanocrystals is expected. EFTEM analysis provides valuable information to this regard, allowing building up a statistical histogram of the nanocrystal size as a function of the introduced Si excess. A systematic increase of the average size of the Si nanograins has been observed when increasing the implantation dose, together with a rather small dispersion around the mean value (0.3-0.5 nm typical). The typical diameters range from 3.6 nm obtained for the sample with the lowest Si excess (7%), to 4.1 nm for the intermediate Si excess (9.5%) and up to 4.6 nm for the largest Si excess (13%). By combining the values of both the measured Si excess and average particles size, an estimate of the density of nanocrystals can be performed., We obtain a density of about $4x10^{18}$ Si nc/cm^3 for all the samples studied here (all the Si excess). The observation by EFTEM imaging that the superficial density of the nanoparticles is quite similar in all kind of samples provides an additional support to this evaluation. Then we can conclude that in the present conditions we have obtained a set of different samples in which the increasing amount of implanted Si has been converted in a population of nanocrystals with the same density but slightly larger sizes.

The characterization of the PL emission of the samples has been also performed. Typical PL spectra are presented in Fig. 2, with an inset showing the evolution of the total integrated PL intensity with the ion dose. The red-shift of the maximum is perfectly consistent with the increase in size that has been measured from EFTEM and is in agreement with the emission coming from band-edge recombination of excitons quantum confined in Si-nc.

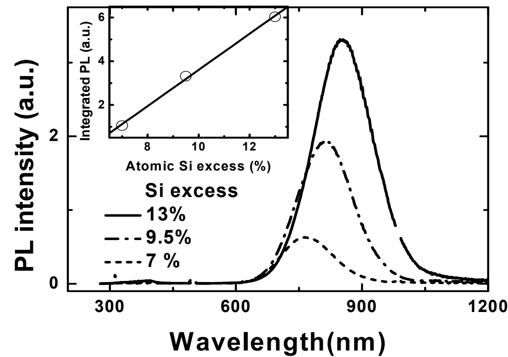

Figure 2. PL spectra of the different implanted and annealed samples. In the inset, the integrated intensity has been plotted as a function of the introduced Si excess.

The values obtained for the maximum of the emission are consistent with values obtained by us in the past from single Si+ ion implants in thermal oxides [5]. Similarly to the results reported in such papers, the PL emission energy peak ranges for the samples studied here between 1.62 eV (lowest dose, 7%) and 1.45 eV (highest dose, 13%). It is also remarkable that the integrated intensity perfectly scales with the Si excess and that higher dose emission spectra overlap those for lower doses in the low wavelength side (high energy). This is apparently due to the fact that the excitation cross-section in the blue-UV-range perfectly scales also with Si excess. So, this scaling is due to the fact that the density of states available for excitation at high energies is proportional to the number of Si excess atoms and not to the density of Si nanocrystals.

In order to evaluate the thickness and refractive index of the active layer, their dependence with the Si excess and original matrix, we performed m-lines measurements. The thickness of the active layer found from m-lines does not depend of the Si excess and is around 340 nm, in good agreement with the values shown before. The refractive index values are presented in Fig. 3 both for pure silica and thermal oxide samples. Thus, by taking the values of refractive index of the composites at 632 nm and the extreme value for x=2 (SiO_2, n=1.46) we can interpolate a dependence of the refractive index with Si excess. This is shown in Fig. 3, which provides very useful data to prepare composite layers with a targeted refractive index.

Efficient propagation of light was observed by coupling a signal both at 633 and 780 nm into the waveguide. Propagation losses measurements have been performed by using both the top-view (light scattering) and the insertion losses technique. The former one is based on the assumption (right in presence of homogeneous surface without irregularities) that the scattered light intensity observed from the top of the waveguide is directly proportional to the light intensity propagating in the waveguide. Hence the decrease of the scattered light as a function of the position along the waveguide is representative of the attenuation of the propagating optical mode and can be easily detected by looking at the top surface of the waveguide with a CCD camera. The image is then acquired by a frame grabber and analysed to obtain the intensity profile as a function of the waveguide length. This approach is not the best for precise measurements of losses coefficients if compared to the usual cut-back method or to insertion losses technique. However, it is a simple, rapid and not sample-consuming technique to have an upper estimation of propagation losses. The latter one, insertion losses technique, is based on the measurement of the power transmitted from the waveguide output facet as a function of the input signal power and needs an

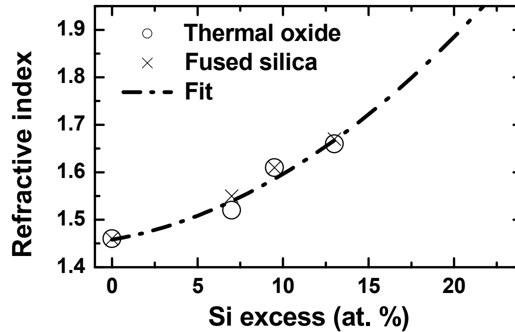

Figure 3. Refractive index of the active layer as a function of the introduced Si excess. The values obtained by M-lines measurements have been interpolated by a polynomial fit.

independent estimation/measurements of the coupling in and collection losses. The losses through the optical collection system have been determined by measuring the transmitted power of the tapered fiber in front of the microscope objective: the value was about 5 dB. Also the tapered fiber losses have been measured in order to know the real power injected into the waveguide. The coupling losses are mainly due to the different numerical aperture between tapered fiber and waveguide sample, to the tapered fiber's focused spot size against waveguide geometrical dimensions, to reflections and edge defects or irregularities. An experimental evaluation of about 15-16 dB has been obtained by a comparison with similar waveguides for which it was possible to determine the propagation losses by cut-back technique, and hence to deduce the coupling losses. An estimation of coupling losses has been made also by calculating the contribution of the various effects, resulting in losses of about 17 dB for the largest waveguide (8 μm), increasing up to 23 dB for the smallest (2 μm).

Fig. 4a shows, as example, the scattered light intensity along the sample length of a 8 μm wide waveguide with 9.5% Si excess. An exponential fit of the data yields a propagation loss coefficient of about 11 dB/cm. Propagation losses coefficients as a function of the rib width have been obtained as mean values of four different waveguides. The values obtained by the top-view measurements have been validated by the insertion losses measurements: the results are in agreement within 1 dB/cm.No significant differences in the propagation loss coefficient have been found by changing the wavelength of the light from 633nm to 780nm. Remarkable differences between the various rib widths can be observed, as shown in Fig. 4b: larger losses, around 20 dB/cm, are present in the small (1 and 2 μm) waveguides, whereas they stabilize around 11 dB/cm in the large ones (4, 6 and 8 μm). This can be mainly attributed to roughness scattering of the side walls of the ridge, together with the loss of confinement, both terms being more predominant when reducing the channel width.

The asymptotic value of about 11 dB/cm, which represents the intrinsic loss due to propagation in the active layer, has been analysed further. Scattering losses from the ensemble of Si previously determined, and result in about 2 dB/cm at 633 nm and 1 dB/cm at 780 nm. If we assume that the remaining 9 dB/cm losses are absorption losses we can get an upper limit estimate to the absorption cross-section for Si-nc, σ_{abs}~$5x10^{-19}$ cm^2. This low value of absorption cross-section

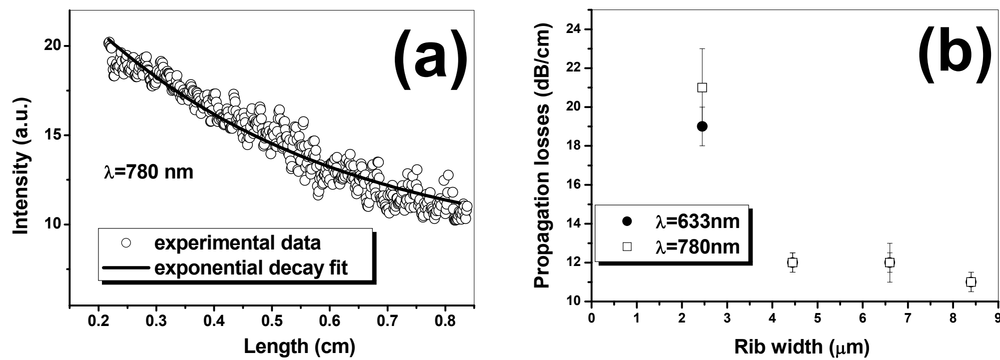

Figure 4. (a) Scattered light intensity (top-view measurements) along the sample length of a 8 μm rib width waveguide at 780 nm. (b) Variation of the propagation losses with rib width at 633nm and 780nm.

is compatible with other reported data and supports the 4-level model for the stimulated emission in Si-nc. If for the stimulated emission cross-section a value of about $1x10^{-17}$ cm^2 is assumed [6], we can get an estimate of the gain coefficient in these waveguides, attainable when the system is pumped with suitable high energy radiation. The ultimate performances of similar, optimized waveguide amplifier under optical pumping should be extremely promising, being just 11 dB/cm losses and a gain coefficient of about 160 dB/cm.

CONCLUSIONS

We have been able to get a deep insight into the formation, loss contributions and mechanisms in waveguides made with Si nanocrystals-rich oxides. An exhaustive characterization of the active layer has been performed in order to control the formation and emission properties of the nanoparticles, and get valuable physical parameters, such as the nanocrystal density and size and refractive index of the multilayer structure. Propagation losses have been measured on the processed waveguides, and related to specific contributions. An asymptotic value, around 2 dB/cm of Mie scattering and 9 dB/cm of direct absorption was evaluated. The feasibility of a highly performance optical amplifier which makes use of similar optimized structures has been suggested.

REFERENCES

1. B. Garrido, M. López, C. García, A. Pérez-Rodríguez, J. R. Morante, C. Bonafos, M. Carrada, A. Claverie, J. Appl. Phys. **91**, 798 (2002).
2. S. Ossicini, L. Pavesi, F. Priolo *Light Emitting Silicon for Microphotonics*, Springer Tracts in Modern Physics , Vol. 194 (Springer-Verlag, Berlin 2003).
3. L. Pavesi, L. Dal Negro, C. Mazzoleni, G. Franzò, F. Priolo, Nature **408**, 440 (2000).
4. J. Ruan, P.M. Fauchet, L. Dal Negro, M. Cazzanelli, L. Pavesi, Appl. Phys. Lett. **83**, 5479 (2003).
5. B. Garrido, M. López, O. González, A. Pérez-Rodríguez, J. R. Morante, C. Bonafos, Appl. Phys. Lett. **77**, 3143 (2000).
6. L. Dal Negro, M. Cazzanelli, N. Daldosso, Z. Gaburro, L. Pavesi, D. Pacifici, G. Franzò, F. Priolo, and F. Iacona, Physica E **16**, 297 (2003).